The Interaction of Katabatic Flow and Mountain Waves. Part I: Observations and Idealized Simulations

GREGORY S. POULOS

Los Alamos National Laboratory, Los Alamos, New Mexico, and Colorado State University, Fort Collins, Colorado

JAMES E. BOSSERT

Los Alamos National Laboratory, Los Alamos, New Mexico

THOMAS B. MCKEE AND ROGER A. PIELKE

Colorado State University, Fort Collins, Colorado

(Manuscript received 13 April 1998, in final form 8 July 1999)

ABSTRACT

The mutual interaction of katabatic flow in the nocturnal boundary layer (NBL) and topographically forced gravity waves is investigated. Due to the nonlinear nature of these phenomena, analysis focuses on information obtained from the 1993 Atmospheric Studies in Complex Terrain field program held at the mountain–canyon–plains interface near Eldorado Canyon, Colorado, and idealized simulations. Perturbations to katabatic flow by mountain waves, relative to their more steady form in quiescent conditions, are found to be caused by dynamic pressure effects. Based on a local Froude number climatology, case study analysis, and the simulations, the dynamic pressure effect is theorized to occur as gravity wave pressure perturbations are transmitted through the atmospheric column to the surface and, through altered horizontal pressure gradient forcing, to the surface-based katabatic flows. It is proposed that these perturbations are a routine feature in the atmospheric record and represent a significant portion of the variability in complex terrain katabatic flows.

The amplitude, wavelength, and vertical structure of mountain waves caused by flow over a barrier are themselves partly determined by the evolving structure of the NBL in which the drainage flows develop. For Froude number Fr $> \sim 0.5$ the mountain wave flow is found to separate from the surface at higher altitudes with NBL evolution (increasing time exposed to radiational cooling), as is expected from Fr considerations. However, flow with Fr $< \sim 0.5$ behaves unexpectedly. In this regime, the separation point descends downslope with NBL evolution. Overall, a highly complicated, mutually evolving, system of mountain wave–katabatic flow interaction is found, such that the two flow phenomena are, at times, indistinguishable. The mechanisms described here are expanded upon in a companion paper through realistic numerical simulations and analysis of a nocturnal case study (3–4 September 1993).

1. Introduction

The investigation of mountain waves and katabatic flows with observational, theoretical, and numerical techniques, has mostly focused on the physics of their generally undisturbed, time-averaged or steady-state characteristics (Jeffreys 1922; Scorer 1949; Defant 1951; Drazin 1961; Thyer 1966; Manins and Sawford 1979; Mahrt 1982; Nappo and Rao 1987; Durran and Klemp 1982; Smolarkiewicz and Rotunno 1989), with some exceptions that are described below. The majority of observational studies, however, reveal the nonidealized nature of these flows; as with most mesoscale phenomena, neither is disconnected from external influences. Still, katabatic flows are a persistent feature over the earth's land and ice masses where any slope exists, and topographically induced gravity waves of some form develop whenever stably stratified flow encounters a barrier. It is the externally induced deviation from an undisturbed state that is investigated here.

Figure 1 from Manins (1992) shows the typical regime for an undisturbed katabatic slope flow. On a slope of angle α, an inversion of depth h develops due to surface radiative cooling and turbulent and radiative transfer of that cooling upwards. The locally colder air near the surface relative to the same height in the free atmosphere creates a pressure gradient sufficient to

Corresponding author address: Gregory S. Poulos, Colorado Research Associates, 3380 Mitchell Lane, Boulder, CO 80301.
E-mail: gsp@co-ra.com

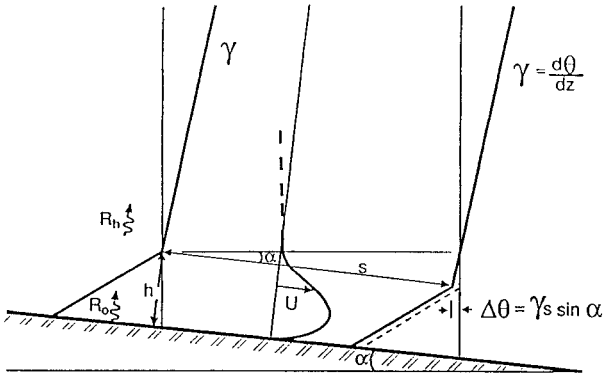

FIG. 1. The conceptual model of katabatic slope flow of Manins (1992). The inversion is drawn for two different slope locations separated by a distance; *s.* Here α is the slope angle, h is the inversion depth, γ is the lapse rate of θ, and u is the downslope wind speed. Also R_h and R_o are the longwave radiative transfer rates of the ground and air aloft, respectively.

cause downslope flow, u (see Hawkes 1947). The greatest temperature deficit and therefore largest pressure gradient is located at the surface. The strongest flow, however, exists some height above ground level due to surface friction retarding the flow near the surface, causing the idealized jet structure. The combination of surface friction and reduced temperature deficit (and pressure gradient) with height produces a jet maximum within the middle third of the inversion depth. Interestingly, a basic dynamical understanding of katabatic flow was given by Fournet (1840) and was later verified by Wenger (1923), Wagner (1932a,b) and Defant (1933) on the strength of circulation theory (Kelvin 1869; Bjerknes 1902). An extensive review of katabatic flow dynamics was given in Poulos (1996), which extends the historical perspective of Hawkes (1947).

Observations of katabatic flow in its natural state indicate a generally unsteady nature (Fig. 3, Cornfeld 1938; Jaffe 1958; Davidson and Rao 1963; Barr and Orgill 1989; Neff and King 1989; Mahrt and Larsen 1990; Orgill et al. 1992; Mursch-Radlgruber 1995; Coulter and Gudiksen 1995; Poulos 1996), even in the most quiescent conditions. In fact, early in the twentieth century A. Defant described an influence of mountain waves on katabatic flow:

> remnants of cold air in valleys form closed systems and may be excited into oscillations (similar to waves on lakes) by the passage of a foehn current over them. These oscillations show up as temperature fluctuations that are not to be confused with the short, periodic pressure fluctuations that occur during foehn (as paraphrased by F. Defant 1951).

This variability can be a serious problem for forecasts of pollutant dispersion, turbulence, and general weather conditions in many regions (Poulos and Bossert 1995), a conclusion theoretically supported by McNider et al. (1995). As noted by Egan (1984), the interaction of katabatic flows with ambient flow is not properly understood. It should also be noted that the physics governing pure slope (inclined plane) katabatic flow, such as investigated by Papadopoulos (1997) and shown in Fig. 1, differs somewhat from that in a canyon where various slope flows converge to form down-canyon (or out canyon, if a level valley floor) katabatic flow (Whiteman 1990).

Mountain wave, or topographically induced internal gravity wave, is the name given to the generic phenomenon of an airflow in a stable atmospheric environment being diverted away from its initially horizontal, barrier-perpendicular path by the barrier (Smith 1979; Baines 1987; Durran 1990). The reaction of the airflow to the barrier changes with velocity, stability, and barrier configuration, often defined by the Froude number (Fr), where $\mathrm{Fr} = U/(NH)$, U is suitably defined wind speed, N is Brunt–Väisälä frequency and H is barrier height. A large body of literature solving various simplified or idealized equation sets for certain parameter spaces exists, as well as a smaller body of observational studies. Although there is some debate, it has been found that linear theory of mountain waves can be successfully applied where $\mathrm{Fr} < 0.1$ and $\mathrm{Fr} > 0.9$ (Queney at al. 1960). If Fr deviates from these ranges, as it frequently does in the Colorado Front Range (see section 2b), the flow behavior is expected to be nonlinear. As in the katabatic flow case, observations are much less ideal than the theory, and much of the published work of late has focused on notable severe mountain wave events (Lilly and Zipser 1972; Lilly 1978; Durran 1986; Scinocca and Peltier 1989; Clark et al. 1994). Whereas these are extreme cases, we hypothesize that the vast majority of realistic cases, albeit much more benign, still have important effects on near-surface wind fields and turbulence.

Research has shown that the atmospheric boundary layer (ABL) strongly affects mountain wave behavior aloft. For example, studies such as Raymond (1972), Ying and Baopu (1993), and Reisner and Smolarkiewicz (1994) have shown that flow over a barrier is increased by a convective boundary layer or surface heating. This effect has recently been shown to alter the vertical structure of mountain wave momentum flux by Chun (1997). Scorer (1967) noted that mountain wave flow may adhere to the topographic surface somewhat more readily during nocturnal cooling, but no discussion of dynamics was given. On the other hand, when studying the impact of mountain waves on boundary layer variability, researchers have mostly focused on so-called ambient flow (Bondy 1935; Barr and Orgill 1989; Gudiksen et al. 1992; Orgill et al. 1992), rather than on mountain waves in particular. When mountain waves are discussed, they are typically more benign mountain waves, instead of the severe mountain waves that cause downslope windstorms (Thomson et al. 1992). In these cases then, boundary layer flow is dominated by thermal forcing (katabatic or anabatic flow) and mesoscale or syn-

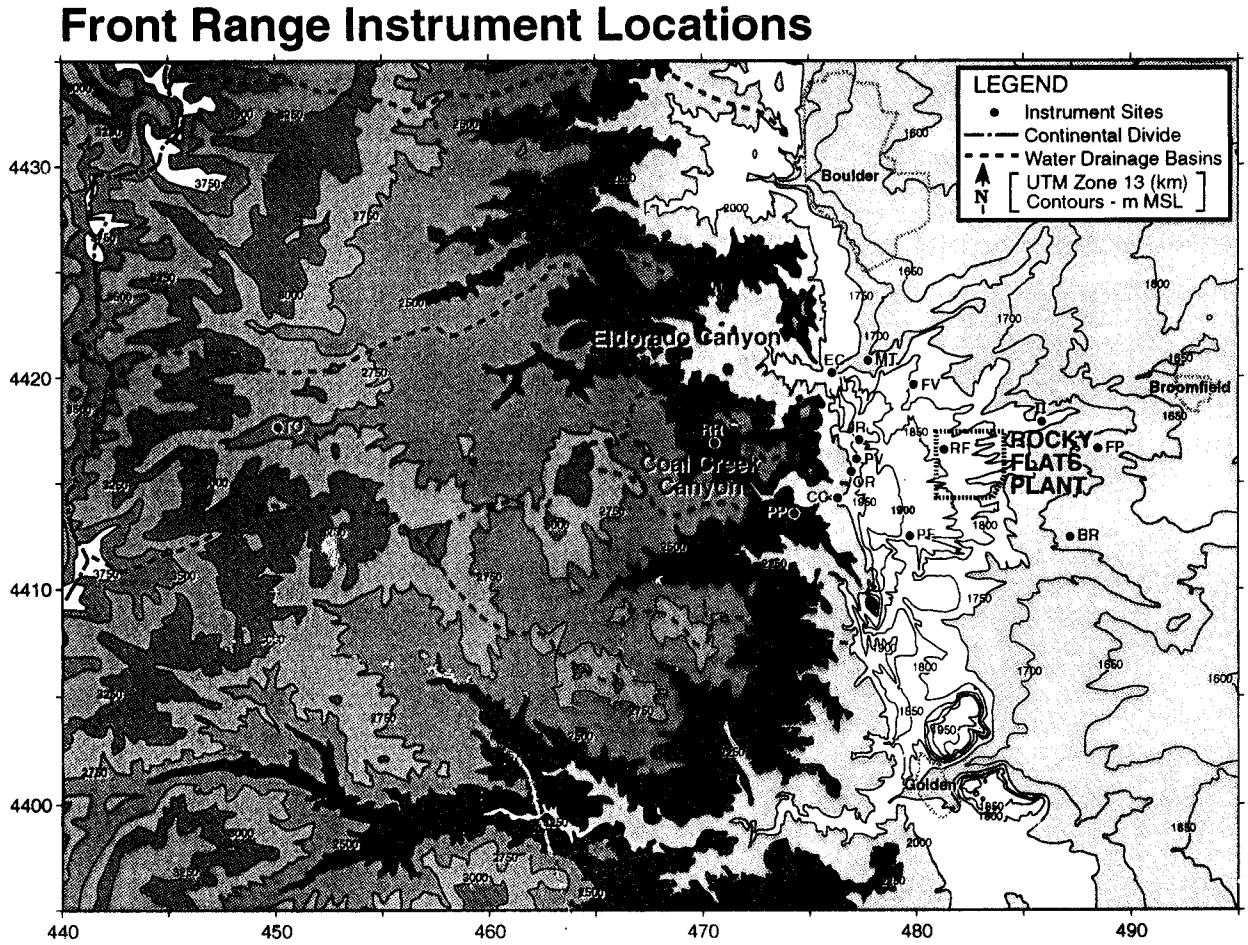

FIG. 2. Observational sites in and around the two main canyons of interest to the 1993 ASCOT experimental campaign in the Front Range of the Colorado Rocky Mountains (courtesy J. Allwine, Pacific Northwest Laboratory). Sites are EC = Eldorado Canyon, CC = Coal Creek Canyon, RF = Rocky Flats, FV = Fairview, RR = Rim Rock, JR = Jim's Ranch, PP = Paul's Peak, PF = Pat's Flat, TO = Tolland, BR = Bartlett, OR = O Ranch, II = Indiana Street, MT = Mine Tower, PV = Pine Valley.

optic pressure gradients, while topographically forced gravity waves propagate aloft, relatively distinct from the boundary layer. Barr and Orgill (1989) found that the depth and strength of katabatic flows in Colorado's Brush Creek Valley were dependent on the local Fr of ambient flow crossing the valley. Wagner (1938), Defant (1951; see quote above), and Mursch-Radlgruber (1995) have noted the possibility of mountain wave–induced pressure perturbations causing some of the ebb and flow in drainage flow observations. Queney (1948) showed that such perturbations can be significant to wind and pressure [$O(1)$ hPa] at the surface, as calculated from linear theory. Ralph et al. (1994), among others, have shown that trapped lee waves also create significant surface perturbations as wave effects are transmitted through the evanescent zone below the ducting layer. Observations have verified that gravity wave–induced perturbations (by either large-scale mountain waves or ducted lee waves) to vertical and horizontal velocity, temperature, and pressure are significant (Lilly and Zipser 1972; Jin et al. 1996). Thomson et al. (1992), using synthetic aperture radar, showed significant influence of ducted lee waves on flow in the marine boundary layer off the coast of Vancouver, Canada.

a. Motivation

This work has its genesis in questions that arise from observational–numerical analysis of katabatic flows from the Atmospheric Studies in Complex Terrain (ASCOT) 1991 field program. During that experiment, an inert tracer was released into the nocturnal, katabatic flow-dominated atmosphere of the mountain–canyon–plains interface near Rocky Flats, Colorado (Fig. 2). The purpose of the numerical modeling that followed was to evaluate the ability of various models to reproduce the measured dispersion of said tracer, with future application to emergency response modeling. In the research that motivated the present work, Poulos and Bossert (1995) noted a significant model bias toward in-

sufficient horizontal dispersion of the modeled tracer relative to observations during thermally stable, nocturnal, katabatic flow conditions. The unexpectedly large horizontal variability of the katabatic flow at this complex terrain site motivated two main questions. What are the mechanisms that create katabatic flow variability? Can a particular natural mechanism be identified as one of the causes of this variability?

b. The hypothesis of MKI

To answer this question, a myriad of wind systems, land-surface characteristics and numerical issues that might influence katabatic flow variability and subsequent tracer dispersion were considered. However, because katabatic and mountain wave flows frequently, and quite often simultaneously, occur in complex topography, it was hypothesized that their mutual interaction would be a likely source of flow variability. This mechanism is termed mountain wave–katabatic flow interaction (MKI) in Poulos (1996) and will also be termed as such in this manuscript. In Part I, here, and Part II, we aim to investigate the concept of mountain wave–katabatic flow interaction. MKI may be manifested as shallower or deeper katabatic layers, stronger or weaker jet speeds, occasional or complete absences of katabatic flow, local gravity wave generation, increased variance of atmospheric fields, or an alteration of layer stability. In turn, the amplitude, wavelength, and vertical structure of the mountain waves themselves is partly determined by the evolving atmospheric stability in which both phenomena reside, resulting in a complex, highly interactive overnight evolution of atmospheric conditions.

We expect that an understanding of MKI could improve 1) local and canyon wind prediction, 2) the understanding of causes of wind variability along mountain ranges, 3) forecasting when ambient flow aloft will descend to the surface, 4) the understanding of leeside layering of wind and temperature fields, and 5) the improvement of diffusion estimates for the thermally stable case in dispersion models. This information is useful to local forecasters, the aviation, the agricultural, and the emergency preparedness–dispersion prediction communities.

c. Organization

This work is described in two parts, Part I (this paper) and Part II, which will appear later. Section 2 of this manuscript contains a description of some meteorological measurements from the 1993 ASCOT field program, including the case study night analyzed in Part II. Section 3 gives a brief overview of the Regional Atmospheric Modeling System (RAMS) and its configuration for this study. Section 4 describes the results of 2D idealized sensitivity simulations, while section 5 discusses the 3D idealized simulations, in brief. The sum of the analyses presented here are used to formulate a preliminary understanding of MKI through discussion in section 6. Part II extends and clarifies the process of MKI with detailed analysis of dynamics, allowing the creation of a conceptual model (Poulos 1996).

2. Observational analysis

Whereas the study that motivated this work was based on field measurements from the 1991 ASCOT experiment (Poulos and Bossert 1995), this work utilizes observations from the ASCOT 1993 field experiment near the Colorado Front Range during the period of August–November 1993 (Fig. 2). There were three primary observing platforms: sodars, wind profilers, and towers. These instruments were placed strategically in and around the two canyons of interest to ASCOT investigators, Coal Creek and Eldorado Canyons. The wind profilers were oriented in a roughly east–west line from just west of the Continental Divide to ~100 km east of the mountain–plains interface to capture larger-scale flow features.

Data from the 10 towers were collected in hourly averages. They were located such that crucial canyon flow information could be obtained (e.g., near canyon heads, canyon mouths, along slopes, etc.), and were mostly instrumented at two levels [typically 6 and 17 m above ground level (AGL)] allowing the determination of low-level stratification. In addition to wind speed, direction, temperature, and relative humidity, most towers also recorded net radiation. Sodars were the primary observational tool for the katabatic flows that developed in the Coal Creek and Eldorado Canyons, although a sodar was not placed in the mouth of Eldorado Canyon (Fig. 2, see also Doran 1996). By recording wind direction, wind speed, and vertical motion with height and time (15 min averages) the sodars allowed continuous monitoring of katabatic flow structure, intrusions from overlying flows, and the twice-daily thermally induced flow transitions. The wind profilers generally retrieved data within a height range of 500–4000 m AGL. The radio acoustic sounding systems co-located with some of the profilers covered a somewhat smaller range from 500 to 2000 m AGL. From the profilers time series of horizontal wind with height were possible, however, numerous data voids prevented the calculation of local Richardson number profiles and the construction of east–west contour plots of profiler winds. In addition to the ASCOT 1993 field campaign data, information from other observational sites, primarily those operated by the National Weather Service (NWS), was obtained. From the 4-month record of ASCOT observational data a single case day is selected to investigate MKI. This case night is simulated and analyzed in Part II.

a. Flow characterization

Clearly, the analysis of case study nights for MKI requires overnight periods where katabatic flow was ev-

ident for some portion of the night. Thus, a katabatic flow ranking system was employed. Throughout the observational period, there exist nights where synoptic or mountain wave forcing completely flushes katabatic winds from a slope or canyon (Pielke 1985; Lee et al. 1987; Lee et el. 1989; Clark et el. 1994; Durran 1986), but since katabatic forcing is not dominant in these cases, such instances are not investigated here. Rather, cases of katabatic flow where the likelihood of mountain wave interaction was high, but not dominant, are sought (Barr and Orgill 1989). An objective and subjective hunt was made through the many days of the ASCOT observational campaign to identify days on which katabatic flow existed, because objective predictors of good katabatic flow nights have been found to be imperfect (Gudiksen 1989). Katabatic flow was evident on over 40% of all case nights, and even the most synoptically quiescent cases indicated a variable katabatic flow evolution. The subjective analysis utilized time–height cross sections from the Coal Creek minisodar to determine whether the flow had evolved in a manner that indicated strong katabatic forcing. The objective ranking scheme used data from the Rim Rock tower site (see Fig. 2) to evaluate conditions conducive to the production of katabatic flows. The case night described below, 3–4 September 1993, was selected because the objective and subjective ranking indicated significant katabatic flow throughout the night.

b. Froude number climatology, 1966–93

Given the integral role of mountain waves in this study, a 28-yr Froude number [$\mathrm{Fr}_u = U/(NH)$] climatology was completed based on the Grand Junction, Colorado, twice daily rawinsondes. That climatology utilized a barrier height, H, of 2000 m, ranging from 2000 m MSL (~500 m AGL in Grand Junction) to 4000 m MSL (the approximate height of the Continental Divide in Colorado). The lowest 500 m AGL above Grand Junction was not used in determining H and Fr because ambient flow was better represented above this height. The mean east–west (barrier perpendicular) flow, $\overline{U}$, and mean Brunt–Väisälä frequency, N, were calculated within this 2000-m layer, where

$$N = \left(\frac{g}{\overline{\theta}} \frac{\partial \theta}{\partial z} \right)^{1/2}, \tag{1}$$

g is the gravitational force, and $\overline{\theta}$ is mean potential temperature in the layer. The mean wind speed used in the numerator of Fr was also calculated using the total wind, V, but was restricted to those days when the flow had a large cross-barrier component (directions between 235° and 315°). Froude numbers calculated using V will be referred to as Fr_v.

The average value of Fr_u, 0.31, was less than half the average Fr_v of 0.63, because of the low bias inherent in the calculation of Fr_u by the inclusion of days where only a weak westerly component existed. Since both average Fr values are below 0.8, it is clear that eastward flowing, subcrest air is typically unable to surmount the Rocky Mountain barrier. This is consistent with the study of blocking by Mayr (1993), who found that westerly flow toward the barrier was blocked 50%–85% of the time. It should be noted that either Fr_u or Fr_v indicate that this flow is typically in a nonlinear regime for mountain waves and will evade analytical solution (Smith 1979). Mayr (1993) also found that blocking west of the Rocky Mountain barrier was caused by a mesoscale high pressure that forms on the upwind side of the barrier, which may influence katabatic flow speeds.

For a given U and H, and the overnight condition where atmospheric stratification, N, increases due to radiative cooling, it is expected that mesoscale high pressure on the upwind side of the barrier will strengthen, as would the downwind mesoscale low pressure, in response to the lowering of Fr (Queney 1948; Smith 1979). Although the increasing stratification reduces the turbulent interaction between developing leeside katabatic flows and mountain wave flow, it also acts to increase the surface pressure perturbation due to the overlying mountain wave felt at the surface. One can reasonably surmise that at some point in a leeside canyon, depending on actual Fr, a local, mountain wave–induced mesolow could perturb local katabatic forcing. Since the location of the mesolow would change as mountain wave wavelength responded to the evolving atmospheric stratification, the location of this effect would also evolve and induce katabatic flow variability.

c. Case night 3–4 September 1993: MKI with 320° flow

The night of 3–4 September 1993 featured a mountain wave embedded in northwesterly flow over the Rocky Mountains, as well as katabatic flows within the ASCOT observational network. Though the wind profiler data were insufficient to determine mountain wave behavior, upstream soundings from Grand Junction were used to calculate the Froude number of flow over the Continental Divide. There was just one significant intrusion of external air to the surface through the katabatic flow measured at the mouth of Coal Creek Canyon, indicating that scouring by the mountain wave did not dominate the nocturnal boundary layer (NBL) in this area. For this reason, and the fact that a reasonably complete observational record was available, this night was chosen as the case study for realistic modeling purposes as will be described in Part II. Based on NWS synoptic maps, a deep low pressure system to the northeast near the Arctic Circle and a high pressure system to the southwest were the cause of geostrophic northwesterly flow aloft. This pattern was in place from 0000 UTC to 1200 UTC, with some slight cold advection at Denver (700-hPa temperatures dropped from 13° to 10°C and those

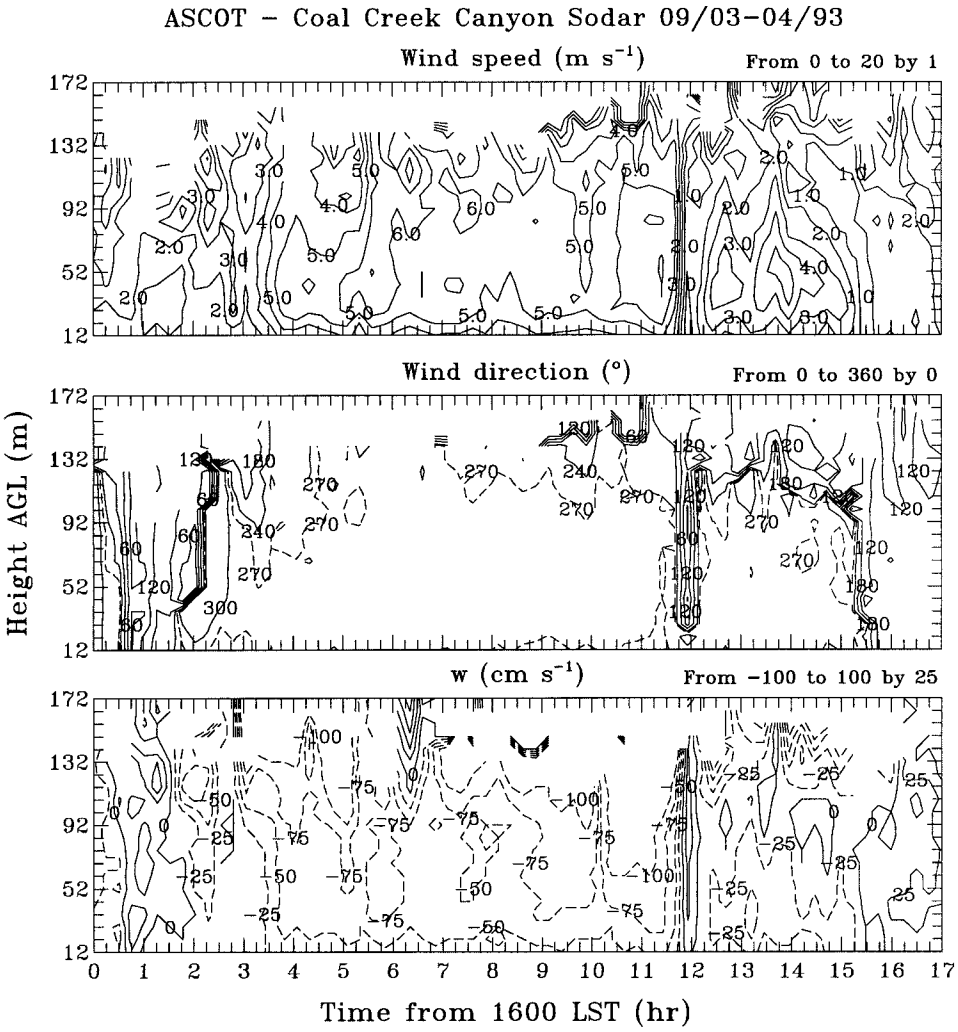

FIG. 3. Coal Creek Canyon sodar observations from 1600 to 0900 LST for (a) wind speed, (b) wind direction, and (c) vertical motion, from the ASCOT 1993 field program for the 3–4 Sep case. Katabatic flow characteristics are clearly shown from the period 1830–0700 LST.

at 500 hPa dropped from −8° to −10°C). Here 850-hPa and surface level plots indicated a slight lee trough over eastern Colorado as expected for such flow. The Grand Junction sounding at 0000 UTC and 1200 UTC showed average flow from 320° at ~7.5 m s^{-1} in the layer from 2000 to 4000 m above mean sea level (MSL). Static stability in this layer averaged ~1.3 K km^{-1} overnight such that Fr = ~0.45 existed for subcrest flow, on average during the period. Since the static stability and vertical wind structure were not constant through this layer, and the Grand Junction sounding does not perfectly represent upstream conditions for the Rocky Mountains, one cannot reasonably presume the existence of the precise mountain wave behavior expected for Fr = 0.45, but rather a generally nonlinear regime response with wave breaking likely at times.

During the day prior to this nighttime case, skies were clear and temperatures reached approximately 30°C with very dry conditions in the Rocky Flats study area; dewpoints were ~0°C. Generally light, southeast, upslope winds existed along the Front Range of the Colorado Rocky Mountains. Overnight, skies remained clear and winds were light and variable at the near surface. Temperatures dropped approximately 19° to 11°C by morning, consistent with strong radiative cooling overnight, and with katabatic flow development in areas sheltered from ambient flow. The tower at Rim Rock, in the upper portion of Coal Creek Canyon (see Fig. 2), indicated that net radiation averaged −67 W m^{-2} from 1800 to 0600 LST (local standard time).

The overnight sodar record from the mouth of Coal Creek Canyon verified katabatic flow development, as shown in Fig. 3, with many of the same features as an undisturbed katabatic flow case. Clearly, this katabatic flow deviates from the ideal, with varying depth, strength, and vertical structure throughout the night.

From Fig. 3a, we note wind lulls both before (1915 LST) and after (0730 LST) the transition to a katabatic flow of at least 165-m depth with jet structure. A sudden reduction in the 5–7 m s^{-1} wind speed and alteration of the wind direction (from 270° to <180°) occurs at 0400 LST that we believe is associated with the intrusion of ambient flow. Given the existence of nonlinear regime, mountain wave flow aloft, and indications of occasional overturning (temporary significant changes in wind direction) from the upstream wind profiler at Gross Reservoir (not shown, see Part II), this intrusion seems to be temporarily penetrative, rotor activity. The well-known transition from upslope to downslope, out-canyon flow (1915 LST), as well as the transition back to upslope flow toward morning (0730 LST) is also shown in Fig. 3b (Wagner 1938; Buettner and Thyer 1965). During the short intrusion at 0400 LST, winds suddenly shift away from the out-canyon direction, and then return to the out-canyon direction with the resumption of katabatic flow. The vertical motion, shown in Fig. 3c, corresponds well to the patterns described above, with positive *w* during upslope and intrusion periods, and subsidence during katabatic flow periods. We believe that evolving mountain wave conditions partly explain the variability of the katabatic flow in this and other cases.

3. Modeling description

To extract the influence of mountain waves on katabatic flows, a series of 2D and 3D simulations were performed. In this idealized numerical laboratory systematic changes in flow characteristics can be observed, particularly as compared to a rapidly changing realistic situation. Three types of simulations were used to determine the significance of MKI: 1) katabatic flow only (KFO, where winds on topography were caused by radiative cooling from an initially zero wind state), 2) mountain wave only (MWO, radiative effects not active) for various Froude number flows, and 3) realistic simulations (the combination of elements 1) and 2) above, referred to as MKI). Comparisons of these sensitivity simulations, despite the unavoidable nonlinearities in the problem, give considerable insight into the influence of mountain waves on katabatic flows [Stein and Alpert (1993), also see section 6.3 of Poulos (1996)]. In all cases the topographic relief was 2000 m and topography was an equilateral barrier. The east and west barrier slopes are $\alpha = 2.5°$, which approximates the average slope of the Front Range from the Continental Divide to the plains near Eldorado Canyon. The mountain therefore approximates an infinite north–south ridge, with slopes that descend to the flat plains on either side. The initially pointed mountain was smoothed once with a four-point smoothing routine to ease the severity of the transition from mountain slope to flat plain and round out the mountain peak. All simulations were run for a 12-h overnight period with radiative conditions, when applied, for the autumnal equinox.

The model used was RAMS version 3a (Pielke et al. 1992), which is a prognostic, nonhydrostatic, primitive equation, mesoscale model developed at Colorado State University. Advective and source terms are time differenced using a basic leapfrog formulation and Asselin filter; turbulent quantities are time differenced using a forward scheme and acoustic terms are time differenced using a forward-backward semi-implicit scheme over a smaller time step than used for the other terms (due to the high speed of sound waves relative to typical atmospheric motions). A thorough description of the various features of RAMS can be found in Pielke et al. (1992) and is not included here.

4. Two-dimensional idealized simulations

A total of nine simulations of varying configuration were completed. One KFO simulation was completed to determine the undisturbed katabatic flow that would develop overnight. Four MWO simulations at Fr = 0.25, 0.50, 0.75, and 1.0, without radiative forcing, were done. Finally, four MKI simulations with both radiative and Fr forcing (again at Fr = 0.25, 0.50, 0.75, and 1.0) were completed. In all cases the horizontal grid spacing was 500 m while the vertical grid spacing was constant at 20 m for 500 m AGL (to resolve katabatic flows). Above 500 m AGL the vertical grid spacing sequentially increased by a factor of 1.1 until reaching a fixed size of 400 m. Domain depth was 10.5 km in the KFO simulation and 17.7 km in the MWO and MKI runs. The higher domain was necessary for runs with flow over the barrier to adequately capture the vertical propagation of mountain waves. Accordingly, the upper-boundary condition was a solid boundary with several Rayleigh-friction absorbing layers, which prevented unrealistic reflection of upward-propagating wave energy. The lower-boundary condition was no-slip and turbulence was parameterized using the standard RAMS scheme, which is a modified form of Smagorinsky (1963) closure.

a. Katabatic flow only (KFO)

This simulation investigates the basic katabatic flow that will develop from initial winds of zero over the mountainside. Static stability was set to 2.5 K km^{-1} in the lowest 3000 m (1000 m above mountaintop) and 3.4 K km^{-1}, the *U.S. Standard Atmosphere,* above that. The following discussion is sufficient to describe the characteristics of the 3D KFO simulation as well, because it was nearly identical to the 2D KFO simulation

As expected, slope-side katabatic flow grows in strength symmetrically over time and by 8 h it has the characteristics shown in Figs. 4a–c, where only the lowest ~1000 m of elevation on the east side of the barrier are shown. Subject to the very idealized initial conditions, the parameterized radiational cooling is very ef-

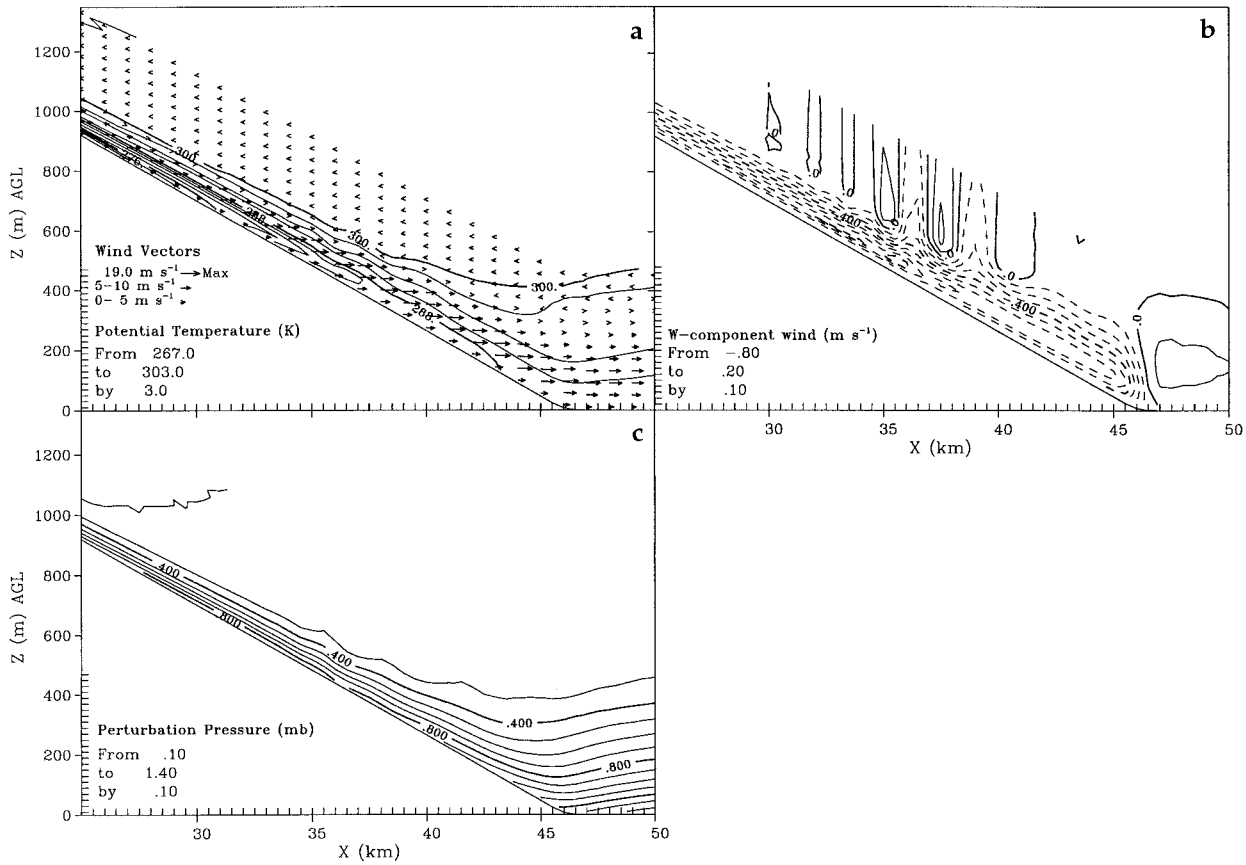

FIG. 4. Model results from the lower portion of the eastern slope in the two-dimensional, 2.5° slope, katabatic flow simulation; (a) θ and wind vectors, (b) vertical motion, and (c) perturbation pressure, for 8 h from model start. Note that these results were symmetric, so that these plots also accurately represent the western slope as well.

fective and causes cooling of ~30°C by this time (Fig. 4a). Consequently, a strong inversion and conditions for strong katabatic flow forcing exist to a degree that would not normally be observed in nature. Over the upper 70% of the slope (partially shown), the katabatic flow increases in depth and speed with distance downslope from the peak, with a jet at 30 m AGL. The peak jet speed, 20.5 m s^{-1}, occurs at 1454 m of vertical drop (x = 36 km), where vertical drop is defined as the vertical distance downward from a horizontal line drawn at the point of highest topography (the standard definition). Within the lowest ~30% of the slope, however, jet speed decreases and jet height increases to 90 m AGL due to upstream effects of the plain (Bossert and Poulos 1995). The katabatic flow depth, defined as the depth at which flow vectors reverse direction, is a nearly constant 0.11 of vertical drop but then deepens, below 1500 m of vertical drop, to as much as 0.16 at the mountain–plains interface (x = 46 km). At that interface, the jet speed has reduced by ~25% of its peak value, the jet height has tripled, and the total flow depth has doubled. The jet deceleration is in response to the reversal of the pressure gradient force on the plains (Fig. 4c). With distance away from the slope on the plain (only partially shown in Fig. 4), katabatic flow reaches a maximum depth of approximately 500 m. The flow structure of both the 2D and 3D katabatic flow only simulations does not change much after 8 h.

A 1–3 m s^{-1} return flow develops aloft (Fig. 4a), agreeing with scant observations of natural katabatic flows when ambient flow is sufficiently quiescent by Buettner and Thyer (1965) and Defant (1951). A pool of cold air begins to accumulate on the flat plain, elevating the jet, resulting in positive vertical motion over the plain (Fig. 4b). Internal gravity waves of wavelength $\lambda \sim 3000$ m form in the shear zone above the jet just below 1000 m of vertical drop. Using the characteristics of this katabatic flow, a depth, $d \sim 200$ m, and Ri ~ 0.2, the λ for these gravity waves is consistent with the formulation derived by Lott (1997), who showed for a stably stratified shear layer that, $\lambda = (2\pi d)/(\sqrt{\text{Ri}})$. When strong enough shear exists in similar simulations with longer slopes, these gravity waves will break, causing Kelvin–Helmholtz billows. The low-level inversion strength is ~80 K km^{-1} at x = 35 km over a height of 150 m and still stronger upstream of this point to as much as 200 K km^{-1}. Although these values seem high, values up to 128 K km^{-1} were observed on towers dur-

ing the ASCOT 1993 experimental program (Poulos 1996). Overall, by nature of the idealized initial condition, the variability of this flow is minimal, and the katabatic forcing quite intense, relative to the observed katabatic flow shown in Fig. 3.

b. Mountain wave only (MWO)

The purpose of these simulations was to define the atmospheric response to a variety of idealized, but realistic, flows over topography. Static stability was initialized as in the KFO simulations. Using this stratification to calculate N, and an H of 1500 m, Fr was defined by setting the wind speed to the appropriate value. A value of 1500 m was used for H, rather than 2000 m, because wind speed was prescribed to be zero at the surface with a linear increase to the selected speed at 500 m above the lowest topography, and constant above that. This was done to be consistent in comparisons with the MKI runs where ambient flow was introduced only after katabatic flow developed to a depth of 500 m.

Each MWO simulation showed strongly accelerated flow on the eastern slope, as depicted in Fig. 5. Compared with their initialized wind speeds of 3.39, 6.78, 10.17, and 13.55 m s^{-1}, respectively, the Fr = 0.25, 0.50, 0.75, and 1.0 simulations accelerate by a maximum factor of 3.24, 2.65, 2.55, and 2.21, respectively, on the eastern slope by 3 h. Due to weaker forcing, mountain waves with successively smaller Fr separate farther up the lee slope. In addition to strong vertical perturbations, the Fr = 0.25 simulation shows low-level return flow and an elevated wave breaking region with poorly defined lee-wave structure. Also in the nonlinear regime, the Fr = 0.50 simulation contains breaking waves aloft and lee waves downstream of the barrier. The Fr = 0.75 simulation contains weak wave breaking aloft but the Fr = 1.00 does not (even at high altitudes not shown in the plot window), whereas significant lee waves exist in both. The Fr = 0.75 simulation shows return flow and other rotor activity at the lowest levels, but the Fr = 1.00 simulation shows only low-level rotor activity. On the western side of the barrier, easterly flow in the Fr = 0.25 and Fr = 0.50 plots shows that blocked flow has developed at the lowest levels, as expected for low Froude number flow. Very weak blocking also appears in the Fr = 0.75. simulation beneath the 0.0 contour, but none occurs in the Fr = 1.00 simulation (Fig. 5d).

The deformation of the initially horizontal θ profile is shown for each simulation in Figs. 5e–h. The vertical θ contours in Figs. 5e–g verify that wave breaking occurs downstream of the barrier for Fr = 0.25 and 0.50 and at higher levels for Fr = 0.75. For Fr = 1.0 the θ contours are nearly vertical in places, but the flow never reverses. The location of wave breaking aloft and the vertical wavelength increases with increasing Fr. The wave separation point, as in Figs. 5a–d, is a smaller distance downslope as Fr decreases. From this behavior it is logical to conclude that higher Fr flow will scour or prevent the development of katabatic flow to a greater distance downslope than lower Fr flow. Additionally, for lower Fr, weak flow will exist on both the up- and downstream sides of the barrier at low levels, where katabatic flow is more likely to form. The pressure perturbations (not shown) within the topographically anchored portion of the wave and the lee waves downstream, are also likely to impart variability to NBL flow; this phenomenon is investigated further in Part II.

c. Mountain wave–katabatic flow interaction (MKI)

To investigate the interaction of mountain waves with katabatic flow, the model configurations of KFO and MWO were combined. Katabatic flow, just as in KFO (Fig. 4), was allowed to develop to approximately steady state (6 h) before ambient flow was linearly increased over 30 min to the wind speed appropriate for the Fr of interest. This wind ''spinup'' was imposed at altitudes > 500 m above the lowest topography. It was therefore assured that katabatic flow was well developed prior to the existence of the mountain wave forcing, such that their interaction might be more easily assessed. This spin-up configuration also was the reason for the use of $H = 1500$ m in the Fr calculations. Figures 6a–h show u component winds and θ for each of the four simulated Fr numbers (0.25, 0.50, 0.75, and 1.00) at 9 h into the simulation. However, since winds were spun up at 6 h into the simulation, the time shown in Fig. 6 is equivalent to the 3-h time in the MWO simulations and is comparable to the plots in Fig. 5.

On the upstream side of the barrier at each Fr, there are significant differences between the mountain wave flow under the influence of radiative cooling (Fig. 6) and that without (Fig. 5). Also, katabatic flow (Fig. 4) is dramatically influenced by all of the Fr simulated, less so with decreasing Fr. In each case, stratification on the west side of the barrier, combined with a favorable pressure gradient, provides an environment where katabatic flow continues, despite opposing ambient flow. Mountain wave downslope winds in the lee are stronger in all but the Fr = 1.0 MKI case, compared to the MWO simulations, showing the influence of radiative cooling on mountain wave flow behavior. Analysis of the individual terms of the u-momentum equation from the simulations (not shown), indicate generally increased eastward pressure gradient force in the MKI simulations. A similar combination of forcings was found by Arritt and Pielke (1986) in a 1D modeling study and in the observations of Mursch–Radlgruber (1995). The stronger near-surface thermal stratification on the western slopes of Figs. 6e–h, compared to that of the MWO simulations (Figs. 5e–h), indicates that katabatic forcing (radiational cooling) is still significant despite the overlying mountain wave. Furthermore, a comparison of the flow for, say, Fr = 0.50, shows that without radiative cooling the upstream, blocked easterly flow measures

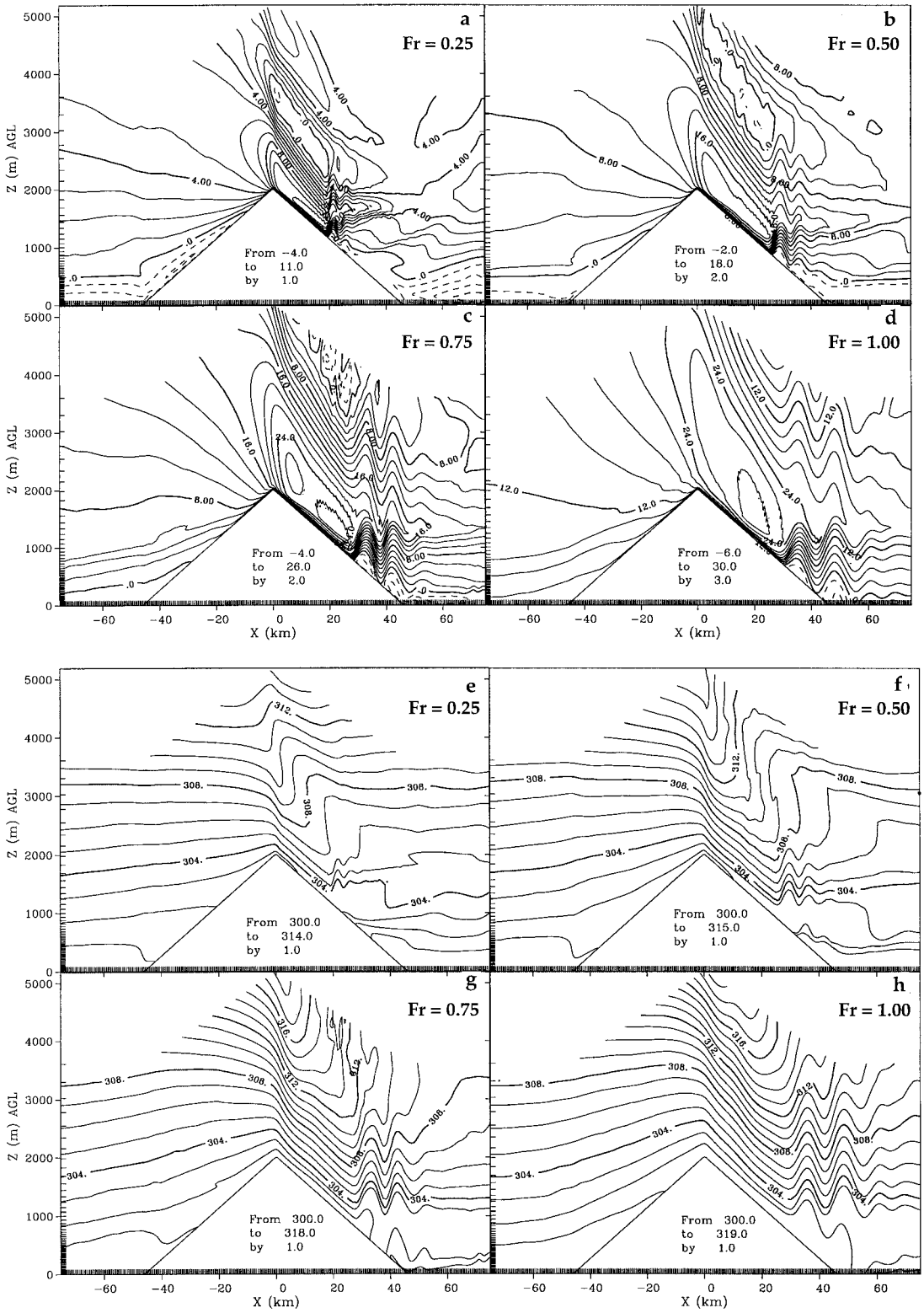

FIG. 5. Here u contours for (a) Fr = 0.25 at 1 m s^{-1} intervals, (b) Fr = 0.50 at 2 m s^{-1} intervals, (c) Fr = 0.75 at 2 m s^{-1} intervals, and (d) Fr = 1.0 at 3 m s^{-1} intervals, and θ contours at 1 K intervals for (e) Fr = 0.25, (f) Fr = 0.50, (g) Fr = 0.75, and (h) Fr = 1.0, at 3 h into the MWO two-dimensional simulations.

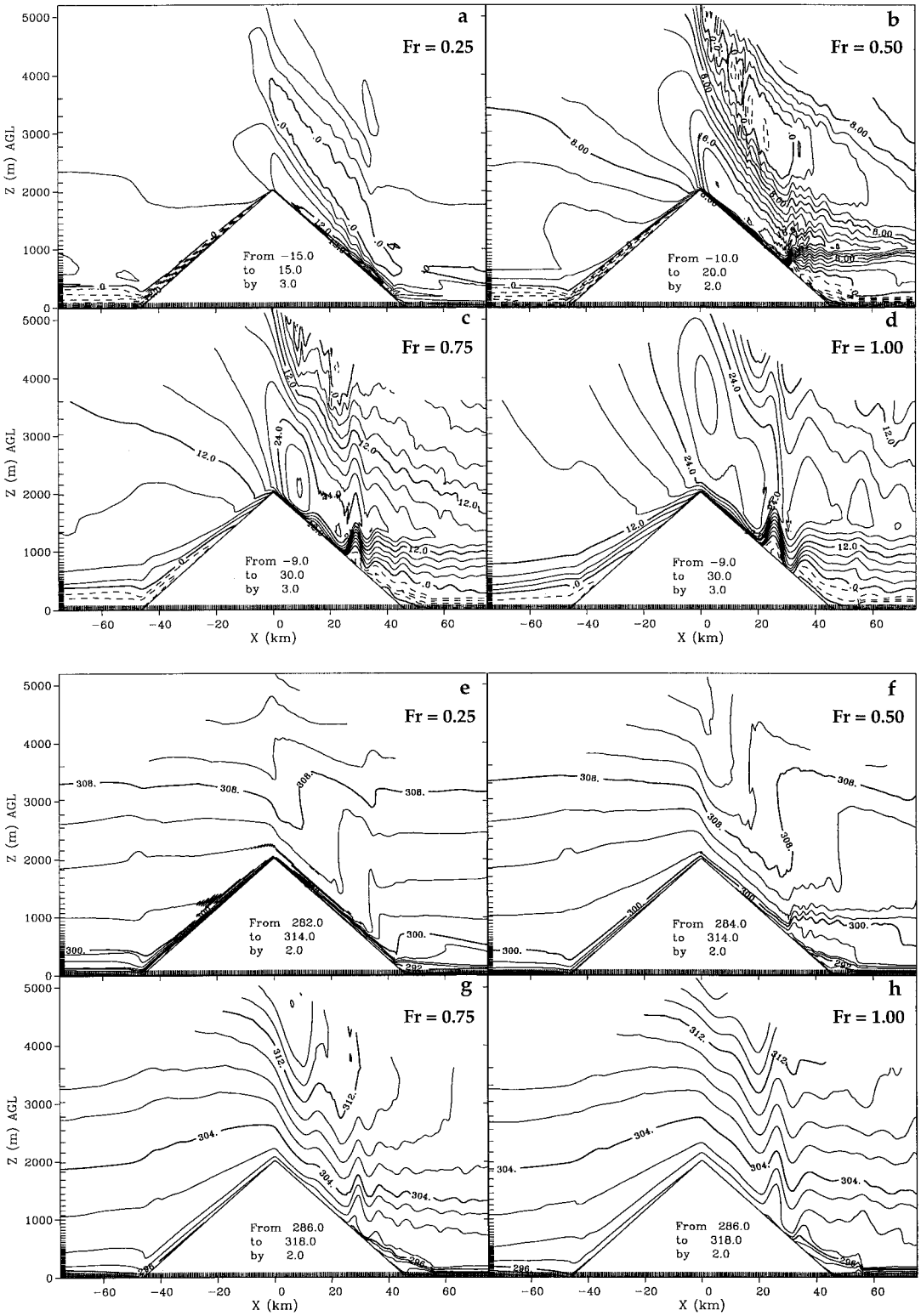

FIG. 6. Here u contours for (a) Fr = 0.25, (b) Fr = 0.50, (c) Fr = 0.75, and (d) Fr = 1.0 and θ contours for (e) Fr = 0.25, (f) Fr = 0.50, (g) Fr = 0.75, and (h) Fr = 1.0 at 9 h into the idealized two-dimensional MKI simulations. The radiation parameterization is active. These panels are comparable in time to the MWO panels shown in Fig. 5.

only $\sim$2 m s^{-1} (Fig. 5b), but with radiative forcing the return flow is as high as $\sim$10 m s^{-1} (Fig. 6b). On the other hand, with only radiative forcing in the KFO simulation the western side flow reaches a greater value, 13.5 m s^{-1} at 9 h (not shown). Similar relationships, though with different magnitudes, are found for each Fr.

Generally the existence of mountain wave flow reduces the strength of the upstream-side katabatic flow that would otherwise exist in quiescent conditions (based on the KFO simulations, see Fig. 4), and this reduction is greater as the strength of flow increases (or Fr increases). We believe this effect can be explained by stronger mixing as Fr increases due to the enhanced shear between the katabatic flow and the ambient flow aloft. This mixing causes $d\theta/dx$ to decrease relative to KFO and, correspondingly, a weaker horizontal pressure gradient force and katabatic flow. On the other hand, the MKI simulations (Fig. 6) show that radiative cooling increases the upstream-side return flow relative to the MWO simulations (see Fig. 5). Note, for the purposes of this discussion, that the mountain wave-induced return flow and the katabatic flow occupy roughly the same physical space in all three types of simulation. The maximum near-surface return flow on the upstream side in the Fr = 0.25 MWO case is ~ -3.0 m s^{-1} (Fig. 5a) and increases to ~ -15.0 m s^{-1} in the Fr = 0.25 MKI case (Fig. 6a), a difference of $\sim$12.0 m s^{-1}. When this difference is calculated for increasing Fr, it decreases to $\sim$7.0 m s^{-1} for Fr = 0.50 (-2.0 m s^{-1} for MWO vs -9.0 m s^{-1} for MKI), $\sim$6.0 m s^{-1} for Fr = 0.75 (-1.0 m s^{-1} for MWO vs -7.0 m s^{-1} for MKI), and to $\sim$50 m s^{-1} for Fr, = 1.0 (1.0 m s^{-1} for MWO vs -4.0 m s^{-1} for MKI). This shows that with increased flow speed or Fr, longwave radiational cooling is less effective in generating pressure gradient force (PGF) in the direction opposing the flow in a nonlinear way. This effect is caused by the decrease in the mountain wave–induced blocking as Fr increases, combined with decreased katabatic forcing due to mixing as Fr increases. The average value of model PGF and turbulent forcing for u velocity at 90 m AGL at $x = -22.75$ km for the MKI simulations reinforces this conclusion; as Fr increases from 0.25 to 1.0, PGF decreases from ~ -0.010 to -0.005 m s^{-2}, and turbulent forcing increases from $\sim$0.001 to 0.003 m s^{-2}. As a result, the easterly flow on the upstream side of the barrier in the MKI simulations can be described as a combination of mountain wave and katabatic forcing.

On the eastern side of the barrier for the MKI simulations (Fig. 6), large differences in flow behavior compared with the MWO simulations (Fig. 5) are found. For MKI and Fr = 0.25 and 0.5 the mountain wave separates from the lee slope farther downslope (cf. Figs. 6a and 6e to Figs. 5a and 5e). Such an effect has been noted by Scorer (1967) without dynamical explanation and is not logically explained by the increasing N, which should lower Fr further. However, it appears from visual inspection of plots of model tendencies of θ (not shown) that radiational cooling of the flow as it descends, restrains vertical lifting of the flow from the lee slope surface. Furthermore, lessened turbulence in these lower Fr flows contributes to this effect by reducing the distribution of cooled near-surface air to significant heights and thus reducing the depth through which N is increased. The stronger near-surface $d\theta/dz$ in Figs. 6e and 6f compared with Figs. 6g and 6h, support this idea. At higher Fr the mountain wave separates from the slope somewhat higher than without radiative cooling. This phenomenon is more intuitively understood than the low Fr effect, because as radiative cooling increases N one would expect a lowering of Fr and, as shown in Fig. 5, a subsequent upslope movement of the separation point. The model tendencies of θ for Fr = 0.75 and 1.00 verify that radiative cooling of the flow is offset by advection of warmer θ air in the high Fr flow.

Returning to our analysis of the Fr = 0.25 case, we see from Fig. 6a that the downward phase of the mountain wave on the eastern side of the mountain has essentially combined with the katabatic flow there. Flow speed along the mountainside is actually stronger than in either MWO or KFO, showing that the momentum of the wave has augmented that of the katabatic flow and the two phenomena seem indistinguishable. This is verified by the continuous stratification on the eastern side seen in Fig. 6e and the presence of modified katabatic flow after 6 h in height versus time plot of u in Fig. 7a. Figure 6e also shows that vertical isentropes exist very near the lowest topography, whereas in Fig. 6e for MWO wave breaking only occurred approximately halfway down the mountainside. Clearly, though both mountain wave and katabatic flow exist in these simulations, their behavior and evolution is drastically changed from what it was as independent entities. In fact, the term katabatic flow no longer seems appropriate terminology to describe the flows on the eastern side, because katabatic-type forcing is only a portion of the dynamical reason for this flow. Time plots (not shown) of the magnitude of u-forcings at $x = 37.25$ km and 90 m AGL for Fr = 0.25 verify that pure katabatic forcing is significantly altered when mountain wave flow aloft is introduced (after 6 h of simulated time), despite the appearance of katabatic-flow-like jet structure (Fig. 7a). Figure 7a shows that Fr = 0.25 flow after 6 h is more variable than prior to 6 h, showing that mountain wave flow induces variability of O[10] min. Furthermore, the speed of the flow jet is reduced and its height is altered. The appearance of this variability is considerably more realistic based upon the appearance of measured katabatic flow in Coal Creek Canyon (Fig. 3).

For higher Fr than 0.25, a return flow toward the barrier occurs in the lee at low levels. In each case, however, this return flow lies above a very shallow layer of weak, variable ($<$3.0 m s^{-1}) katabatic flow. Thus, strong near-surface thermal stability has provided a favorable environment for katabatic flows at low eleva-

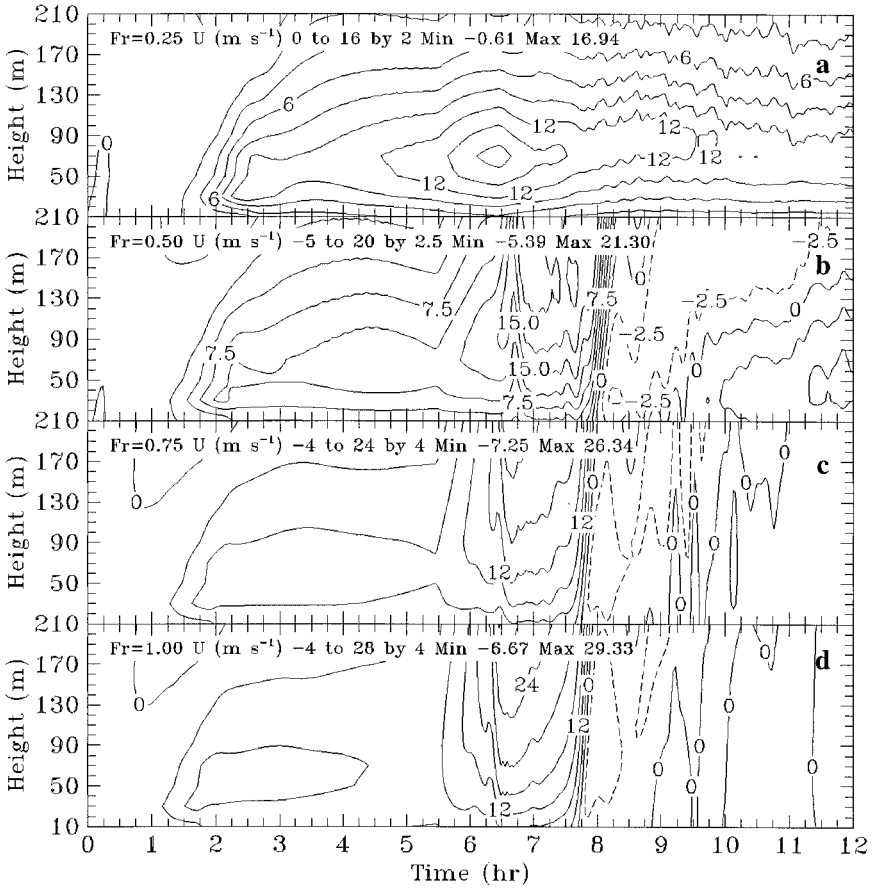

FIG. 7. Height vs time contours of u velocity for each of the 4 MKI simulations at $x = 37.25$ km (80% of the distance down the lee slope). The full 12 h simulation is shown for Fr = (a) 0.25, (b) 0.50, (c) 0.75, and (d) 1.0. The first 6 h show a katabatic jet flow structure, and mountain flow forcing is imposed at 6 h over a half-hour period. Katabatic flow is always present for Fr = 0.25, reestablished at ~ 9 h for the other Fr (though weakly for Fr = 0.75 and 1.00.)

tions despite the destructive influence of mountain wave momentum. It is notable that in Fig. 7b, for Fr = 0.50 at a location 80% of the distance down the lee slope, that katabatic-flow-like structure is reestablished after ~9.5 h as radiatively cooled layers are able to deepen. Figures 7c and 8d, for Fr = 0.75 and 1.00, respectively, show that while positive u flow exists at later times it is weak and variable. In contrast, along the upper slopes katabatic flow has been completely scoured, and flow there is dominated by mountain wave momentum. (Figs. 8b–d show scouring occurs from ~h 6–8 until radiatively driven stable layers again develop, resulting in greatly reduced windspeeds.) Thus, MKI results in 180° wind direction change depending on when mountain wave forcing penetrates to the surface or not. These simulations cannot be analyzed for wind direction changes out of the east–west plane. Thermal stability in these upper altitudes is smaller as the strength of the scouring momentum or size of Fr, increases (see near-surface θ on Figs. 6e–g). It is intriguing to note that for Fr = 0.50 the scouring of katabatic flow occurs farther downslope than for higher Fr at this simulation time. At altitudes less than the wave separation point, weaker flow and stronger thermal stability develop (e.g., Figs. 8b–d after ~8 h). The lee-wave structure in the Fr = 0.75 and Fr = 1.00 cases has also been altered compared to the MWO simulations by the inclusion of radiative cooling, with implications for gustiness.

At 12 h, or 6 h after the beginning of full mountain wave forcing, the flow has evolved to a considerably different form compared with Fig. 6, as shown in Fig. 8. For Fr = 0.25 (Figs. 6a and 8a), continued radiative cooling has driven stronger katabatic flows on the western side than at 9 h, but those on the eastern side are approximately the same (see also Fig. 7a). The mountain wave structure is still embedded within the stable layers that also generate the katabatic flow. Waves continue to break on the eastern side, but due to increased stratification, the location of the lowest significant downslope separation point (from $x = 35$ km in Fig. 6 to $x = \sim 25$ km, where vertical isentropes rise vertically ~1 km) has moved uphill. The stronger stratification has restricted

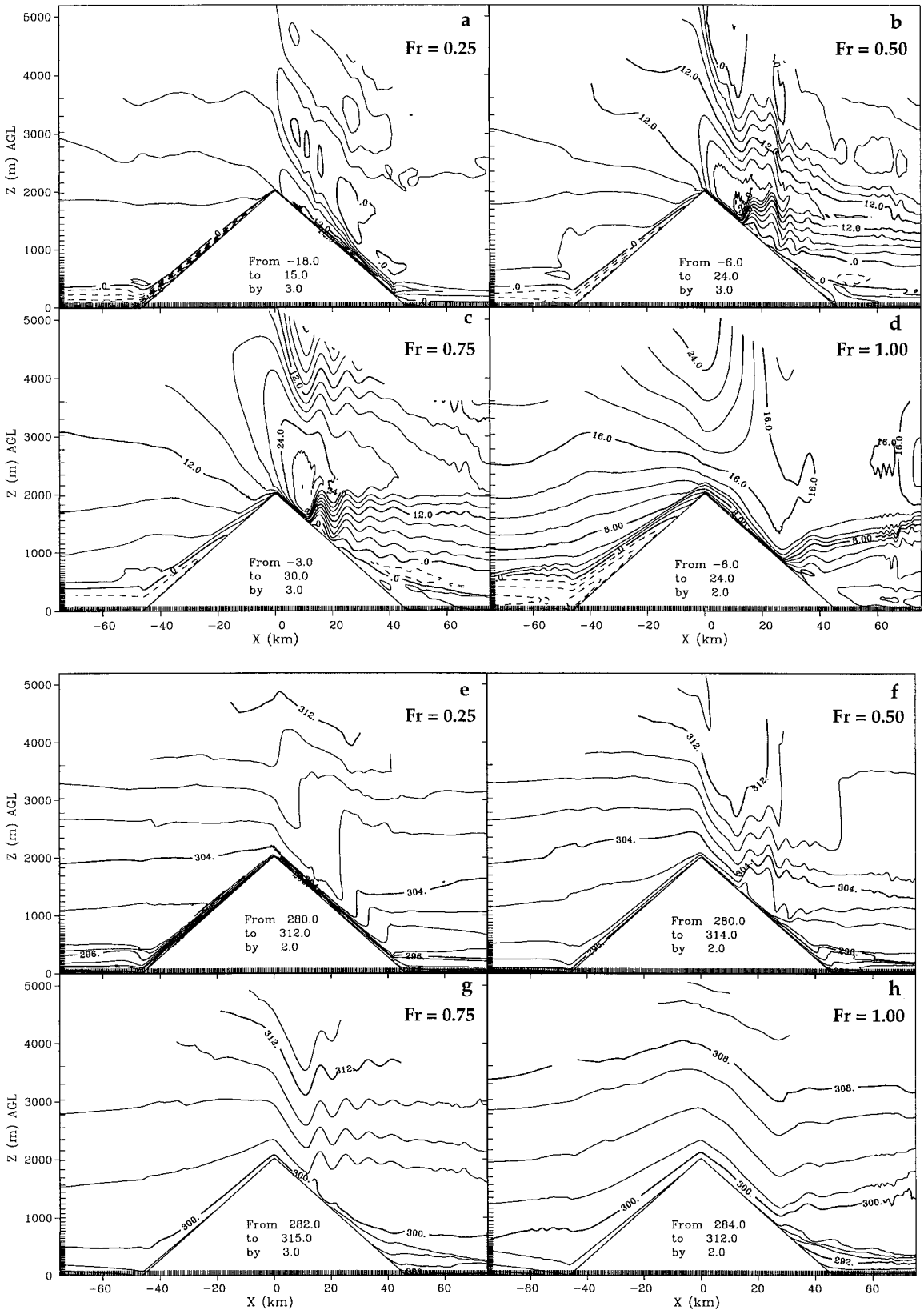

FIG. 8. As in Fig. 6, but for 12 h into the idealized 2D MKI simulations.

the penetration depth of the mountain wave resulting in the separation point of the Fr = 0.50 and 0.75 waves being shifted upstream significantly from their 9-h position, though the wave for Fr = 0.50 still separates at a lower altitude than for Fr = 0.75. Accordingly, katabatic flow develops in the relatively quiescent zone underlying this separation point for Fr = 0.75, as shown in Fig. 7c after 9 h. Due to the deepened katabatic flow associated with deepened alongslope stratification for Fr = 0.5 and 0.75, return flow is restricted to a smaller vertical layer, is weaker and less continuous than at 9 h.

For Fr = 1.0 in Figs. 8d and 8h, lee waves have completely disappeared from the mountain wave structure but the separation point remains nearly halfway down the mountain. Despite the fact that for Fr = 1.0 stable stratification overlays a less stable zone on the eastern side of the peak at 9 and 12 h (Figs. 6 and 8), at 12 h this stratification is weaker (as is flow speed), resulting in a poorer ducting condition, and thus the elimination of lee waves. Similar to the other Froude numbers, low-level stable layers on the eastern side of the barrier are deeper due to continued radiative cooling with a shear-driven nearly neutral layer above. Return flow has disappeared (see also Fig. 7d) most likely due to a combination of subsequently stronger katabatic forcing and weakened overlying flow. Strengthening of katabatic flow due to radiative cooling and flow deceleration for Fr = 1.0 is most obvious on the western side, where katabatic flow is twice as strong as that at 9 h and has penetrated to higher altitudes resulting in 180° flow direction change.

5. Three-dimensional idealized simulations

Three-dimensional versions of the KFO, MWO, and MKI simulations were also completed, but only for the Fr = 0.50 case. It can be argued that 2D simulations are insufficient to describe the complicated interaction of mountain waves with katabatic flow. This argument is based on theory, which shows that in 2D, turbulence can transfer energy upscale, whereas in 3D upscale transfer is typically small, with the overall effect being downscale energy transfer (Kraichnan 1976). To simulate the natural world then, particularly a turbulent phenomenon such as MKI, would require three dimensions to provide realistic results of detailed flow (Fritts et al. 1996; Afanasyev and Peltier 1998). However, even in our 2D simulations, turbulent dissipation is primarily introduced via a parameterization, a parameterization that dissipates energy regardless of dimension, so we expect that they may perform reasonably well if the subgrid-scale 3D processes are in large part represented by the parameterization. It has already been explained that the 3D KFO simulation was nearly indistinguishable from the 2D KFO simulation, but katabatic flow is typically less turbulent than mountain wave flow. Thus, we may expect more significant differences between 2D and 3D simulations as mountain wave forcing is added. The configuration of the 3D simulation is exactly like its 2D, Fr = 0.50 counterpart, except that 21 grid points have been added in the north–south direction with cyclic boundary conditions (Δy = 500 m).

The results of these simulations were very similar to their 2D counterparts, despite some of the expected cross-slope variability, as shown in Figs. 9a–d, which are comparable to Figs. 5 and 7, respectively. The reader can see that, indeed, these model results compare very closely to the 2D simulations. Temporally, the similarities remain, so that the description of the 2D simulations in the prior section also adequately describes MKI in 3D for these idealized cases. Of course, when realistic orography is included very significant differences exist between two- and three-dimensional simulations. Realistic topography simulations of the ASCOT case night described in section 2c are completed in Part II.

6. Summary and discussion

This work demonstrates, through the use of observational analysis and idealized simulations, that the mountain wave–katabatic flow interaction (MKI) mechanism is robust and significant. Our results show that the interaction is mutually interdependent (i.e., nonlinear). That is, while turbulence and pressure effects imposed on katabatic flows by mountain waves alter their structure, characteristics, and evolution, those same changes (particularly alterations to atmospheric stability) feedback and alter gravity wave evolution, to the point where these two phenomena are indistinguishable. These results are clarified and expanded upon with the detailed dynamic analysis of a high-resolution numerical simulation of the case study night described here (section 2c) in Part II.

a. Influences of MKI on katabatic flow

Though generally katabatic flows have been studied as an entity protected from external forcing by strong thermal stratification, observations here from the ASCOT 1993 field program and other studies show them to contain significant externally induced variability. From the observations (Fig. 3) it appears that intrusions into katabatic flow by breaking or attenuating mountain waves are manifested as alterations in the flow speed and direction (see section 2c). Although drainage flow is partially eroded, it is regenerated after the intrusion and upper-level influence does not prevent the evening and morning transition periods from occurring. Thus, while mountain wave forcing can be sufficient to influence the complex terrain–canyon drainage flows of the region, its influence was not strong enough to significantly affect the surface diurnal cycle. Of course, stronger or higher Fr flow could completely eliminate (or scour) drainage flows in this canyon for the whole overnight period and reach the surface on the plains as well. This effect is only partially addressed in the simulations

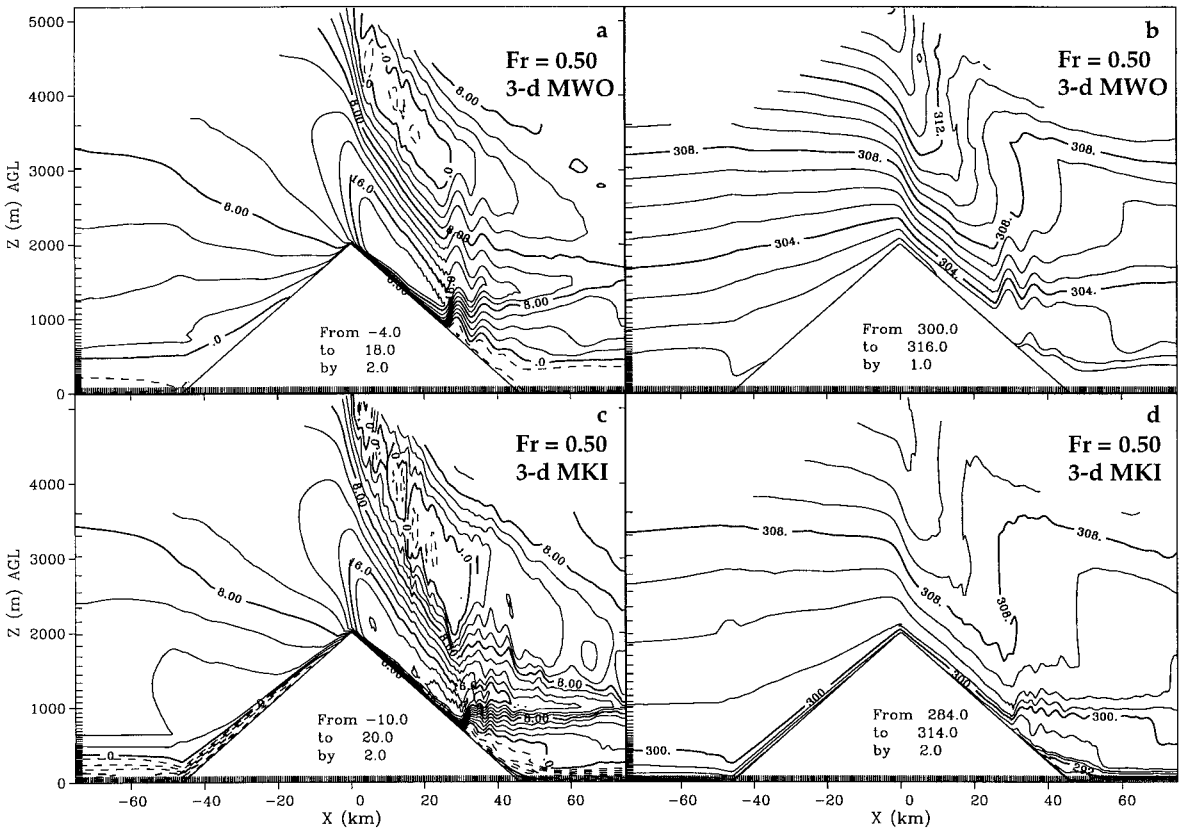

FIG. 9. East–west vertical cross sections through the center of the 3D, idealized, Fr = 0.50, MWO simulation at 3 h for (a) u, comparable to Fig. 5b; (b) θ, comparable to Fig. 5f. (c) and (d) Vertical cross sections through the center of the 3D, idealized, Fr = 0.50, MKI simulation at 9 h. (c) The u contours, comparable to Fig. 6b. (d) The θ contours, comparable to Fig. 6f.

where analysis is done in the east–west plane. In the simulations, katabatic flow exists (does not exist) when mountain wave forcing does not (does) penetrate to the surface, resulting in wind direction changes of 180°. It is difficult to categorize these flows as strictly katabatic flow or mountain wave flow in this complex interaction.

From the idealized numerical simulations a number of other MKI characteristics relevant to katabatic flow were identified. While strong nocturnal stratification was able to develop despite the presence of mountain wave flow on the upstream side of the barrier (which was enhanced by the near-surface, dynamic pressure increase as a consequence of blocking), it was generally weaker than that found without wave forcing due to turbulent mixing of cold air. Such a phenomenon may have been measured by Mursch-Radlgruber (1995). For $0.5 < \text{Fr} < 1.0$, on the downstream side of the barrier but upstream of the mountain wave separation point, katabatic flow is scoured as the mountain wave flow penetrates to the surface although radiative cooling continues. For smaller Fr, such as 0.25, the downslope phase of the mountain wave is found to couple with the katabatic flow, and even enhance its speed. Overall, a temporally variable state is found where mountain waves and katabatic flow interact. Since the Froude number climatology showed that Fr is generally between 0.2 and 0.7, the likelihood of mountain wave–katabatic flow interaction in mountainous regions is high and should be significant.

These results also suggest that dynamic pressure forcing from the overlying mountain wave influences katabatic flow. From the known characteristics of gravity waves (Queney 1948; Grubisic and Smolarkiewicz 1997), topographically forced gravity waves cause a surface pressure perturbation that will vary with terrain shape, atmospheric stability, and wind speed. Gravity waves aloft cause a pressure perturbation that is exponentially evanescent away from the source region. Thus, pressure changes over a barrier caused by a mountain wave or lee waves can locally change the pressure gradient force. Since katabatic flow is dependent on radiatively driven cooling and the subsequent horizontal pressure gradient, the pressure gradient imposed by the gravity wave will influence katabatic flow speeds as our analysis of model forcings verified. Also, changing stratification, wind speed and wind direction overnight can interact with complex topography to cause an evolution in the strength and location of these effects. These ideas are further tested in Part II.

b. Influences of MKI on mountain waves

The idealized simulations also show that the evolving, radiatively driven, nocturnal boundary layer (NBL) in which katabatic flows develop also influences mountain waves, resulting in a complicated, nonlinear, mutual evolution. For smaller Fr, such as 0.25, the downslope phase of the mountain wave is found to couple with the katabatic flow and even enhance its speed. Also, at Fr $<\sim 0.50$, the mountain wave under the influence of radiative cooling is found to have a lower-elevation separation point, as Scorer (1967) suggested may happen. This effect is explained by 1) the effective radiative cooling of low-level mountain wave flow, which restrains the vertical lifting of the flow from the lee slope, and 2) the less efficient mixing of this cooled air upward, which prevents a significant increase in *N*. Interestingly, for Fr $> \sim 0.50$, the mountain wave separation point is higher than it would be if radiative cooling were not occurring. The latter effect is logical as increasing stratification will in turn increase *N*, which will decrease Fr (see section 2b), and we have shown that with lower Fr the separation point is further uphill (Fig. 5). Also, mountain wave flow speed in the lee was found to be enhanced by radiative cooling up to Fr = 0.75. The ASCOT 1993 field program did not contain adequate data for an analysis of these effects directly.

The realistic case night simulations in Part II, allow us to further verify these conclusions and test our hypotheses about the dynamic pressure mechanism of MKI, resulting in a conceptual model.

Acknowledgments. We gratefully acknowledge the Atmospheric Studies in Complex Terrain Program sponsored by the U.S. Department of Energy for supporting this work. A portion was also supported under National Science Foundation Grant ATM-9713073. In addition, we note numerous enlightening discussions regarding this work with Drs. J. T. Lee, Sumner Barr, Bill Porch, Keeley Costigan, and Jon Reisner of Los Alamos National Laboratory; Professors Dick Johnson and Jorge Ramirez and Drs. Mel Nicholls and Bob Walko of Colorado State University; Drs. Mike Weissbluth and Craig Tremback of ASTeR Inc.; Dr. Mike Meyers of the National Weather Service, Grand Junction; Drs. Doug Wesley, Terry Clark, and Piotr Smolarkiewicz of the National Center for Atmospheric Research; Drs. Dave Whiteman and Chris Doran of Pacific Northwest Laboratory; Dr. Jerry Schmidt of the Naval Research Laboratory; Dr. John Snook of the NOAA Forecast Systems Laboratory; Dr. Marty Ralph of the NOAA Environmental Technology Laboratory; Dr. Dick McNider of the University of Alabama; and Dr. Ray Arritt of the University of Iowa.

REFERENCES

Afanasyev, Y. D., and W. R. Peltier, 1998: The three-dimensionalization of stratified flow over two-dimensional topography. *J. Atmos. Sci.,* **55,** 19–39.

Arritt, R. W., and R. A. Pielke, 1986: Interactions of nocturnal slope flows with ambient winds. *Bound.-Layer Meteor.,* **37,** 183–195.

Baines, P. G., 1987: Upstream blocking and airflow over mountains. *Ann. Rev. Fluid Mech.,* **19,** 75–97.

Barr, S., and M. M. Orgill, 1989: Influence of external meteorology on nocturnal valley drainage winds. *J. Appl. Meteor.,* **28,** 497–517.

Bjerknes, V., 1902: Zirkulation relativ zu der Erde. *Meteor. Z.,* **19,** 97–108.

Bondy, F., 1935: Uber beziehungen zwischen periodischen talwinden und verschiedenen meteorologischen faktoren (Relationships between periodic valley winds and various meteorological factors). Ph.D. dissertation, University of Innsbruck, 79 pp. [Available from University of Innsbruck, Institute of Meteorology and Geophysics, Innrain 52, A-6020, Innsbruck, Austria.]

Bossert, J. E., and G. S. Poulos, 1995: A numerical investigation of mechanisms affecting drainage flows in highly complex terrain. *Theor. Appl. Climatol.,* **52,** 119–134.

Buettner, K. J. K., and N. Thyer, 1965: Valley winds in the Mount Rainier area. *Arch. Meteor. Geophys. Bioklimatol.,* **14,** H. 2, 125–147.

Chun, H.-Y., 1997: Weakly non-linear response of a stably stratified shear flow to thermal forcing. *Tellus,* **49A,** 528–543.

Clark, T. L., W. D. Hall, and R. M. Banta, 1994: Two- and three-dimensional simulations of the 9 January 1989 severe Boulder windstorm: Comparison with observations. *J. Atmos. Sci.,* **51,** 2317–2343.

Cornfeld, C. E., 1938: Katabatic winds and the prevention of frost damage. *Quart. J. Roy. Meteor. Soc.,* **64,** 553–584.

Coulter, R. L., and P. Gudiksen, 1995: The dependence of canyon winds and surface cooling and external forcing in Colorado's Front Range. *J. Appl. Meteor.,* **34,** 1419–1429.

Davidson, B., and P. K. Rao, 1963: Experimental studies of the valley-plain wind. *Int. J. Air Water Pollut.,* **7,** 907–923.

Defant, A., 1933: Der abfluss schwerer luftmassen auf geneigten boden, nebst einigen bemerkungen zur theorie stationarer luftstrome (The flow of heavy air masses down slopes along with some remarks on the theory of stationary air currents). *Sitz. Berichte Preuss. Akad. Wiss. Phys.-Math.-Klasse,* **18,** 624–635.

——, 1951: Local winds. *Compendium of Meteorology,* T. F. Malone, Ed., Amer. Meteor. Soc., 655–672.

Doran, J. C., 1996: The influence of canyon winds on flow fields near Colorado's Front Range. *J. Appl. Meteor.,* **35,** 1936–1953.

Drazin, P. G., 1961: On the steady flow of a fluid of variable density past an obstacle. *Tellus,* **13,** 239–251.

Durran, D. R., 1986: Another look at downslope windstorms. Part I: The development of analogs to supercritical flow in an infinitely deep, continuously stratified fluid. *J. Atmos. Sci.,* **43,** 2527–2543.

——, 1990: Mountain waves and downslope winds. *Atmospheric Processes over Complex Terrain, Meteor. Monogr.* No. 45, Amer. Meteor. Soc., 59–81.

——, and J. B. Klemp, 1982: On the effects of moisture on the Brunt–Väisälä frequency. *J. Atmos. Sci.,* **39,** 2152–2158.

Egan, B. A., 1984: Transport and diffusion in complex terrain (a review). *Bound.-Layer Meteor.,* **30,** 3–28.

Fournet, M. J., 1840: Des brises de jour et de nuit autour des montagnes (Daytime and nighttime winds around mountains). *Ann. Chim. Phys.,***74,** 337–401.

Fritts, D. C., T. L. Palmer, O. Andreassen, and I. Lie, 1996: Evolution and breakdown of Kelvin–Helmholtz billows in stratified compressible flows. Part I: Comparison of two- and three-dimensional flows. *J. Atmos. Sci.,* **53,** 3173–3191.

Grubisic, V., and P. K. Smolarkiewicz, 1997: The effect of critical levels on 3D orographic flows: Linear regime. *J. Atmos. Sci.,* **54,** 1943–1960.

Gudiksen, P. H., 1989: Categorization of nocturnal drainage flows within the Brush Creek Valley and the variability of σ_θ in complex terrain. *J. Appl. Meteor.,* **28,** 489–495.

——, J. M. Leone, C. W. King, D. Ruffieux, and W. D. Neff, 1992: Measurements and modeling of the effects of ambient meteo-

rology on nocturnal drainage flows. *J. Appl. Meteor.*, **31,** 1023–1032.
Hawkes, H. B., 1947: Mountain and valley winds with special reference to the diurnal mountain winds of the Great Salt Lake Region. Ph.D. dissertation, Ohio State University, 312 pp. [Available from Department of Geography, Ohio State University, Columbus, OH 43210.]
Jaffe, S., 1958: Effect of prevailing wind on the valley wind regime at anemometer level, preliminary report on valley wind studies in Vermont. AFCRC-TR-58-29, Air Force Cambridge Research Laboratory, 32 pp. [Available from Air Force Research Laboratory, Hanscom Air Force Base, MA 01731.]
Jeffreys, H., 1922: On the dynamics of wind. *Quart. J. Roy. Meteor. Soc.*, **48,** 29–48.
Jin, Y., S. E. Koch, Y-L. Lin, F. M. Ralph, and C. Chen, 1996: Numerical simulations of an observed gravity current and gravity waves in an environment characterized by complex stratification and shear. *J. Atmos. Sci.*, **53,** 3570–3588.
Kelvin, Lord, 1869: On stationary waves in flowing water. *Philos. Mag.*, **5,** 353–357.
Kraichnan, R. H., 1976: Eddy viscosity in two and three dimensions. *J. Atmos. Sci.*, **33,** 1521–1536.
Lee, J. T., R. E. Lawson Jr., and G. L. Marsh, 1987: Flow visualization experiments on stably stratified flow over ridges and valleys. *Meteor. Atmos. Phys.*, **37,** 183–194.
——, R. A. Pielke, R. C. Kessler, and J. Weaver, 1989: Influence of cold pools downstream of mountain barriers on downslope winds and flushing. *Mon. Wea. Rev.*, **117,** 2041–2058.
Lilly, D. K., 1978: A severe downslope windstorm and aircraft turbulence event induced by a mountain wave. *J. Atmos. Sci.*, **35,** 59–77.
——, and E. J. Zipser, 1972: The front range windstorm of 11 January 1972—A meteorological narrative. *Weatherwise*, **25,** 56–63.
Lott, F., 1997: The transient emission of propagating gravity waves by a stably stratified shear layer. *Quart. J. Roy. Meteor. Soc.*, **123,** 1603–1619.
Mahrt, L., 1982: Momentum balance of gravity flows. *J. Atmos. Sci.*, **39,** 2701–2711.
——, and S. Larsen, 1990: Relation of slope winds to the ambient flow over gentle terrain. *Bound.-Layer Meteor.*, **53,** 93–102.
Manins, P. C., 1992: Vertical fluxes in katabatic flows. *Bound.-Layer Meteor.*, **60,** 169–178.
——, and B. L. Sawford, 1979: A model of katabatic winds. *J. Atmos. Sci.*, **36,** 619–630.
Mayr, G. J., 1993: The evolution of orogenic blocking. Ph.D. dissertation, Colorado State University, 131 pp. [Available from Colorado State University, Department of Atmospheric Science, Fort Collins, CO 80523.]
McNider, R. T., D. E. England, M. J. Friedman, and X. Shi, 1995: Predictability of the stable atmospheric boundary layer. *J. Atmos. Sci.*, **52,** 1602–1617.
Mursch-Radlgruber, E., 1995: Observations of flow structure in a small forested valley system. *Theor. Appl. Climatol.*, **52,** 3–17.
Nappo, C. J., and K. S. Rao, 1987: A model study of pure katabatic flows. *Tellus*, **39A,** 61–71.
Neff, W. D., and C. W. King, 1989: Observations of complex terrain flows using acoustic sounders: Drainage flow structure and evolution. *Bound.-Layer Meteor.*, **43,** 15–41.
Orgill, M. M., J. D. Kincheloe, and R. A. Sutherland, 1992: Mesoscale influences on nocturnal valley drainage winds in Western Colorado valleys. *J. Appl. Meteor.*, **31,** 121–141.
Papadopoulos, K. H., C. G. Helmis, A. T. Soilemes, J. Kalogiros, P. G. Papageorgas, and D. N. Asimakopoulos, 1997: The structure of katabatic flows down a simple slope. *Quart. J. Roy. Meteor. Soc.*, **123,** 1581–1601.
Pielke, R. A., 1985: The use of mesoscale numerical models to assess wind distribution and boundary layer structure in complex terrain. *Bound.-Layer Meteor.*, **31,** 217–231.
——, and Coauthors, 1992: A comprehensive meteorological modeling system—RAMS. *Meteor. Atmos. Phys.*, **49,** 69–91.
Poulos, G. S., 1996: The interaction of katabatic winds and mountain waves., Ph.D. dissertation, Colorado State University, 297 pp. [Available from Los Alamos National Laboratory, Publication LA-13224-T, Los Alamos, NM 87545.]
——, and J. E. Bossert, 1995: An observational and prognostic numerical investigation of complex terrain dispersion. *J. Appl. Meteor.*, **34,** 650–669.
Queney, P., 1948: The problem of air flow over mountains: A summary of theoretical studies. *Bull. Amer. Meteor. Soc.*, **29,** 16–26.
——, G. A. Corby, N. Gerbier, H. Koschmieder, and J. Zierep, 1960: The airflow over mountains. Tech. Note 34, World Meteorological Organization, Geneva, Switzerland.
Ralph, F. M., P. J. Neiman, and T. L. Keller, 1994: Nonstationary trapped lee waves. Preprints, *Third Int. Symp. on Tropospheric Profiling: Needs and Technologies*, Hamburg, Germany, European Geophysical Union, 171–174.
Raymond, D. J., 1972: Calculation of airflow over an arbitrary ridge including diabatic heating and cooling. *J. Atmos. Sci.*, **29,** 837–843.
Reisner, J. M., and P. K. Smolarkiewicz, 1994: Thermally forced low Froude number flow past three-dimensional obstacles. *J. Atmos. Sci.*, **51,** 117–133.
Scinocca, J. F., and W. R. Peltier, 1989: Pulsating downslope windstorms. *J. Atmos. Sci.*, **46,** 2885–2914.
Scorer, R. S., 1949: Theory of waves in the lee of mountains. *Quart. J. Roy. Meteor. Soc.*, **75,** 41–56.
——, 1967: Causes and consequences of standing waves. *Proc. Symp. on Mountain Meteorology*, Fort Collins, CO, Colorado State University, 65–67.
Smagorinsky, J., 1963: General circulation experiments with the primitive equations I. The basic experiment. *Mon. Wea. Rev.*, **91,** 99–152.
Smith, R. B., 1979: The influence of mountains on the atmosphere. *Advances in Geophysics*, Vol. 21. Academic Press, 87–230.
Smolarkiewicz, P. K., and R. Rotunno, 1989: Low Froude number flow past three dimensional obstacles. Part I: Baroclinically generated lee vortices. *J. Atmos. Sci.*, **46,** 1154–1164.
Stein, U., and P. Alpert, 1993: Factor separation in numerical simulations. *J. Atmos. Sci.*, **50,** 2107–2115.
Thomson, R. E., P. W. Vachon, and G. A. Borstad, 1992: Airborne synthetic aperture radar imagery of atmospheric gravity waves. *J. Geophys. Res.* **97** (D), 14 249–14 257.
Thyer, N. H., 1966: A theoretical explanation of mountain and valley winds by a numerical method. *Arch. Meteor. Geophys. Bioklimatol.*, **A15,** 318–348.
Wagner, A., 1932a: Hangwind-ausgleichsstroemung-berg und talwind (Slope wind - equalizing flow-mountain and valley wind). *Meteor. Z.*, **49,** 209–217.
——, 1932b: Neue theorie der berg und talwinde (New theory of mountain and valley winds). *Meteor. Z.*, **49,** 329–341.
——, 1938: Theorie und beobachtung der periodischen gebirgswinde (Theory and observation of periodic mountain winds). *Beitr. Geophys.*, **52,** 408–449.
Wenger, R., 1923: Zur theorie der berg-und talwinde (Theory of the mountain and valley wind). *Meteor. Z.*, **40,** 193–204.
Whiteman, C. D., 1990: Observations of thermally developed wind systems in mountainous terrain. *Atmospheric Processes over Complex Terrain, Meteor. Monogr.*, No. 45, Amer. Meteor. Soc., 5–42.
——, C. D., and J. C. Doran, 1993: The relationship between overlying synoptic-scale flows and winds within a valley. *J. Appl. Meteor.*, **32,** 1669–1682.
Ying, Q., and F. Baopu, 1993: A theoretical study on the interaction between airflow over a mountain and the atmospheric boundary layer. *Bound.-Layer Meteor.*, **64,** 101–126.